

Measurement of the $e^+e^- \rightarrow D^{(*)+}D^{(*)-}$ cross-sections

T. Ugllov,¹⁰ K. Abe,⁶ K. Abe,³⁷ T. Abe,⁶ H. Aihara,³⁹ M. Akatsu,¹⁸ Y. Asano,⁴³ T. Aso,⁴² V. Aulchenko,¹ A. M. Bakich,³⁴ Y. Ban,²⁸ U. Bitenc,¹¹ I. Bizjak,¹¹ A. Bondar,¹ A. Bozek,²² M. Bračko,^{17,11} T. E. Browder,⁵ Y. Chao,²¹ B. G. Cheon,³³ R. Chistov,¹⁰ S.-K. Choi,⁴ Y. Choi,³³ A. Chuvikov,²⁹ S. Cole,³⁴ M. Danilov,¹⁰ A. Drutskoy,¹⁰ S. Eidelman,¹ V. Eiges,¹⁰ Y. Enari,¹⁸ D. Epifanov,¹ S. Fratina,¹¹ N. Gabyshev,⁶ A. Garmash,²⁹ T. Gershon,⁶ B. Golob,^{16,11} N. C. Hastings,⁶ H. Hayashii,¹⁹ M. Hazumi,⁶ T. Hokuue,¹⁸ Y. Hoshi,³⁷ H.-C. Huang,²¹ K. Inami,¹⁸ A. Ishikawa,⁶ H. Iwasaki,⁶ M. Iwasaki,³⁹ Y. Iwasaki,⁶ J. H. Kang,⁴⁶ J. S. Kang,¹³ P. Kapusta,²² N. Katayama,⁶ H. Kawai,² T. Kawasaki,²⁴ H. Kichimi,⁶ H. J. Kim,⁴⁶ J. H. Kim,³³ S. K. Kim,³² K. Kinoshita,⁴⁷ P. Koppenburg,⁶ S. Korpar,^{17,11} P. Krokovny,¹ S. Kumar,²⁷ A. Kuzmin,¹ Y.-J. Kwon,⁴⁶ J. S. Lange,^{3,30} G. Leder,⁹ S. H. Lee,³² T. Lesiak,²² J. Li,³¹ S.-W. Lin,²¹ D. Liventsev,¹⁰ J. MacNaughton,⁹ G. Majumder,³⁵ H. Matsumoto,²⁴ T. Matsumoto,⁴⁰ A. Matyja,²² W. Mitaroff,⁹ H. Miyake,²⁶ H. Miyata,²⁴ D. Mohapatra,⁴⁴ T. Nagamine,³⁸ Y. Nagasaka,⁷ T. Nakadaira,³⁹ E. Nakano,²⁵ M. Nakao,⁶ S. Nishida,⁶ O. Nitoh,⁴¹ T. Nozaki,⁶ S. Ogawa,³⁶ T. Ohshima,¹⁸ S. Okuno,¹² S. L. Olsen,⁵ W. Ostrowicz,²² H. Ozaki,⁶ P. Pakhlov,¹⁰ H. Palka,²² C. W. Park,¹³ H. Park,¹⁴ N. Parslow,³⁴ L. S. Peak,³⁴ L. E. Piilonen,⁴⁴ Y. Sakai,⁶ O. Schneider,¹⁵ J. Schümann,²¹ C. Schwanda,⁹ S. Semenov,¹⁰ K. Senyo,¹⁸ R. Seuster,⁵ H. Shibuya,³⁶ B. Shwartz,¹ V. Sidorov,¹ J. B. Singh,²⁷ N. Soni,²⁷ R. Stamen,⁶ S. Stanič,^{43,*} M. Starič,¹¹ T. Sumiyoshi,⁴⁰ S. Suzuki,⁴⁵ O. Tajima,³⁸ F. Takasaki,⁶ K. Tamai,⁶ N. Tamura,²⁴ M. Tanaka,⁶ Y. Teramoto,²⁵ T. Tomura,³⁹ T. Tsuboyama,⁶ T. Tsukamoto,⁶ S. Uehara,⁶ Y. Unno,² S. Uno,⁶ G. Varner,⁵ K. E. Varvell,³⁴ C. C. Wang,²¹ C. H. Wang,²⁰ L. Widhalm,⁹ B. D. Yabsley,⁴⁴ Y. Yamada,⁶ A. Yamaguchi,³⁸ Y. Yamashita,²³ M. Yamauchi,⁶ Heyoung Yang,³² J. Ying,²⁸ Y. Yusa,³⁸ C. C. Zhang,⁸ V. Zhilich,¹ and D. Žontar^{16,11}

(The Belle Collaboration)

¹*Budker Institute of Nuclear Physics, Novosibirsk*

²*Chiba University, Chiba*

³*University of Frankfurt, Frankfurt*

⁴*Gyeongsang National University, Chinju*

⁵*University of Hawaii, Honolulu, Hawaii 96822*

⁶*High Energy Accelerator Research Organization (KEK), Tsukuba*

⁷*Hiroshima Institute of Technology, Hiroshima*

⁸*Institute of High Energy Physics, Chinese Academy of Sciences, Beijing*

⁹*Institute of High Energy Physics, Vienna*

¹⁰*Institute for Theoretical and Experimental Physics, Moscow*

¹¹*J. Stefan Institute, Ljubljana*

¹²*Kanagawa University, Yokohama*

¹³*Korea University, Seoul*

¹⁴*Kyungpook National University, Taegu*

¹⁵*Swiss Federal Institute of Technology of Lausanne, EPFL, Lausanne*

¹⁶*University of Ljubljana, Ljubljana*

¹⁷*University of Maribor, Maribor*

¹⁸*Nagoya University, Nagoya*

¹⁹*Nara Women's University, Nara*

²⁰*National United University, Miao Li*

²¹*Department of Physics, National Taiwan University, Taipei*

²²*H. Niewodniczanski Institute of Nuclear Physics, Krakow*

²³*Nihon Dental College, Niigata*

²⁴*Niigata University, Niigata*

²⁵*Osaka City University, Osaka*

²⁶*Osaka University, Osaka*

²⁷*Panjab University, Chandigarh*

²⁸*Peking University, Beijing*

²⁹*Princeton University, Princeton, New Jersey 08545*

³⁰*RIKEN BNL Research Center, Upton, New York 11973*

³¹*University of Science and Technology of China, Hefei*

³²*Seoul National University, Seoul*

³³*Sungkyunkwan University, Suwon*

³⁴University of Sydney, Sydney NSW

³⁵Tata Institute of Fundamental Research, Bombay

³⁶Toho University, Funabashi

³⁷Tohoku Gakuin University, Tagajo

³⁸Tohoku University, Sendai

³⁹Department of Physics, University of Tokyo, Tokyo

⁴⁰Tokyo Metropolitan University, Tokyo

⁴¹Tokyo University of Agriculture and Technology, Tokyo

⁴²Toyama National College of Maritime Technology, Toyama

⁴³University of Tsukuba, Tsukuba

⁴⁴Virginia Polytechnic Institute and State University, Blacksburg, Virginia 24061

⁴⁵Yokkaichi University, Yokkaichi

⁴⁶Yonsei University, Seoul

⁴⁷University of Cincinnati, Cincinnati, Ohio 45221

We report first measurements of $e^+e^- \rightarrow D^{(*)+}D^{(*)-}$ processes far above threshold. The cross-sections for $e^+e^- \rightarrow D_T^{*+}D_L^{*-}$ and $e^+e^- \rightarrow D^+D_T^{*-}$ at $\sqrt{s} = 10.58 \text{ GeV}/c^2$ are measured to be $0.55 \pm 0.03 \pm 0.05 \text{ pb}$ and $0.62 \pm 0.03 \pm 0.06 \text{ pb}$, respectively. We set upper limits on the cross-sections for $e^+e^- \rightarrow D_T^{*+}D_T^{*-}$, $e^+e^- \rightarrow D_L^{*+}D_L^{*-}$, $e^+e^- \rightarrow D^+D_L^{*-}$ and $e^+e^- \rightarrow D^+D^-$ processes. The analysis is based on 88.9 fb^{-1} of data collected by the Belle experiment at the KEKB e^+e^- asymmetric collider.

PACS numbers: 13.65.+i, 12.38.Hg, 13.87.Fh

The processes $e^+e^- \rightarrow D^{(*)}\bar{D}^{(*)}$, with no extra fragmentation particles in the final state, have not previously been measured for energies $\sqrt{s} \gg 2M_D$. The cross-sections for these processes can be computed once the charmed meson form factors are determined for the appropriate value of momentum transfer, $q^2 \equiv s$. In the HQET approach based on the heavy-quark spin symmetry, the heavy meson form factors can be expressed in terms of a universal form factor, called the Isgur-Wise function. However, for large q^2 , the leading-twist contribution, which violates heavy-quark spin symmetry, becomes dominant [1]. For an intermediate range of momentum transfer, the Isgur-Wise contribution (having subleading twist) is also important. A calculation that takes these effects into account [1] predicts that the cross sections for $e^+e^- \rightarrow D\bar{D}^*$ and $e^+e^- \rightarrow D_L^*\bar{D}_T^*$ are equal to each other, and are about 2.5 pb at $\sqrt{s} \sim 10.6 \text{ GeV}$ (the subscripts indicate longitudinal [L] and transverse [T] polarizations of the D^*). The cross-section for $e^+e^- \rightarrow D\bar{D}$ is expected to be suppressed by a factor of $\sim 10^{-3}$. The cross-section predictions are subject to large uncertainties (\sim a factor of 3), because the theoretical formulae contain many poorly known parameters; the prediction that the $D\bar{D}^*$ and $D_L^*\bar{D}_T^*$ cross-sections should be equal is expected to be robust [2]. Recently, new calculations in the framework of the constituent quark model have become available [3].

In this paper, we present the first measurement of the $e^+e^- \rightarrow D^{*+}D^{*-}$ and $e^+e^- \rightarrow D^+D^{*-}$ cross-sections and polarizations at $\sqrt{s} \sim 10.6 \text{ GeV}$. We also set an upper limit on the cross-section for $e^+e^- \rightarrow D^+D^-$. The present study is limited to final states that contain charged $D^{(*)}$ mesons only. Since the contribution of the electromagnetic current coupled to light quarks is negli-

gible compared to that for heavy quarks, the neutral and charged charm meson cross-sections are expected to be the same [1].

The analysis is based on 88.9 fb^{-1} of data at the $\Upsilon(4S)$ resonance and nearby continuum, collected with the Belle detector [4] at the KEKB asymmetric energy e^+e^- collider [5]. We select well-reconstructed tracks consistent with originating from the interaction region as charged pion candidates. Those passing particle identification cuts based on dE/dx , aerogel Čerenkov, and time-of-flight information [4] are selected as charged kaon candidates. We then reconstruct D^0 and D^+ mesons in the decay modes $D^0 \rightarrow K^-\pi^+$, $D^0 \rightarrow K^-\pi^+\pi^+\pi^-$ and $D^+ \rightarrow K^-\pi^+\pi^+$. The selected combinations are constrained to a common vertex, and quality cuts are imposed on the vertex fit to reduce the combinatorial background. A 15 MeV/ c^2 interval around the nominal D masses is used to select $D^0 \rightarrow K^-\pi^+$ and $D^+ \rightarrow K^-\pi^+\pi^+$ candidates; for the $D^0 \rightarrow K^-\pi^+\pi^+\pi^-$ decay mode the signal window is chosen to be 10 MeV/ c^2 around the nominal D^0 mass ($\sim 2\sigma$ each case). The selected D candidates are then subjected to a mass and vertex constrained fit to improve their momentum resolution. The D^{*+} mesons are reconstructed in the $D^0\pi^+$ decay mode. The mass of the $D^0\pi^+$ combination is required to be within a 2 MeV/ c^2 ($\sim 3\sigma$) mass interval around the nominal D^{*+} mass.

The processes $e^+e^- \rightarrow D^{(*)+}D^{(*)-}$ can be identified by energy-momentum balance in fully reconstructed events that contain only a pair of charm mesons. However, the small charm meson reconstruction efficiency of the studied channels results in a tiny total efficiency in this case. Because of the simple two-body kinematics, it is sufficient to reconstruct only one of the two charmed

mesons in the event to identify the processes of interest. For simplicity, we refer to the fully reconstructed D meson as the $D^{(*)+}$, and the other as the D^{*-} ; the charge-conjugate modes are included in the analysis. We choose the mass of the system recoiling against the reconstructed $D^{(*)+}$ ($M_{\text{recoil}}(D^{(*)+})$) as a discriminating variable: $M_{\text{recoil}}(D^{(*)+}) = \sqrt{(\sqrt{s} - E_{D^{(*)+}})^2 - \vec{p}_{D^{(*)+}}^2}$, where \sqrt{s} is the total center of mass (CM) energy, and $E_{D^{(*)+}}$ and $\vec{p}_{D^{(*)+}}$ are the CM energy and momentum of the reconstructed $D^{(*)+}$. For the signal, a peak in the M_{recoil} distribution around the nominal D^- or D^{*-} mass is expected. This method provides a significantly increased efficiency, but also a higher background, in comparison with full event reconstruction. For the $e^+e^- \rightarrow D^+D^{*-}$ and $e^+e^- \rightarrow D^{*+}D^{*-}$ processes we find a better compromise between higher statistics and smaller background: the first $D^{(*)+}$ is fully reconstructed, while the recoiling D^{*-} is required to decay into $\bar{D}^0\pi_{\text{slow}}^-$. The reconstructed π_{slow}^- provides extra information that allows us to reduce the background to a negligible level using the difference between the masses of the systems recoiling against the $D^{(*)+}\pi_{\text{slow}}^-$ combination, and against the $D^{(*)+}$ alone, $\Delta M_{\text{recoil}} \equiv M_{\text{recoil}}(D^{(*)+}) - M_{\text{recoil}}(D^{(*)+}\pi_{\text{slow}}^-)$. The variable ΔM_{recoil} peaks around the nominal $D^{*-} - \bar{D}^0$ mass difference with a resolution of $\sigma_{\Delta M_{\text{recoil}}} \sim 1 \text{ MeV}/c^2$ as found by Monte Carlo (MC) simulation. For $e^+e^- \rightarrow D^{*+}D^{*-}$ and $e^+e^- \rightarrow D^+D^{*-}$ we require ΔM_{recoil} to be within a $\pm 2 \text{ MeV}/c^2$ interval around the nominal $M_{D^{*-}} - M_{\bar{D}^0}$ mass difference.

The $M_{\text{recoil}}(D^{*+})$ and $M_{\text{recoil}}(D^+)$ distributions are shown in Figs. 1a and 1b, respectively. Clear signals are seen around the nominal D^{*-} mass in both cases. The higher recoil mass tails in the signal distributions are due to initial state radiation (*ISR*). The M_{recoil} distributions for events in the ΔM_{recoil} sideband ($0.150 \text{ MeV}/c^2 < \Delta M_{\text{recoil}} < 0.154 \text{ MeV}/c^2$) are shown as the hatched histogram (barely visible in Fig. 1a due to its small size).

The backgrounds in the region $M_{\text{recoil}} < 2.1 \text{ GeV}/c^2$ are negligible for both processes, so we consider this interval as the signal region. There are three possible background sources:

- I incorrectly reconstructed D^{*+} or D^+ ;
- II $e^+e^- \rightarrow D^{(*)+}Dn\pi^-$ ($n \geq 0$), where the π_{slow}^- is not produced from D^{*-} decay (and can be either from fragmentation or from unreconstructed D decay), and thus produces no peak in the ΔM_{recoil} distribution;
- III $e^+e^- \rightarrow D^{(*)+}D^{*-}n\pi$, where $n \geq 1$.

First we consider the process $e^+e^- \rightarrow D^{*+}D^{*-}$. To estimate background (I) numerically, we count the entries in the signal region for $D^0\pi^+$ combinations taken from the D^{*+} mass sideband ($2.016 \text{ GeV}/c^2 < M_{D^0\pi^+} < 2.020 \text{ GeV}/c^2$). Three events are found in the data, while

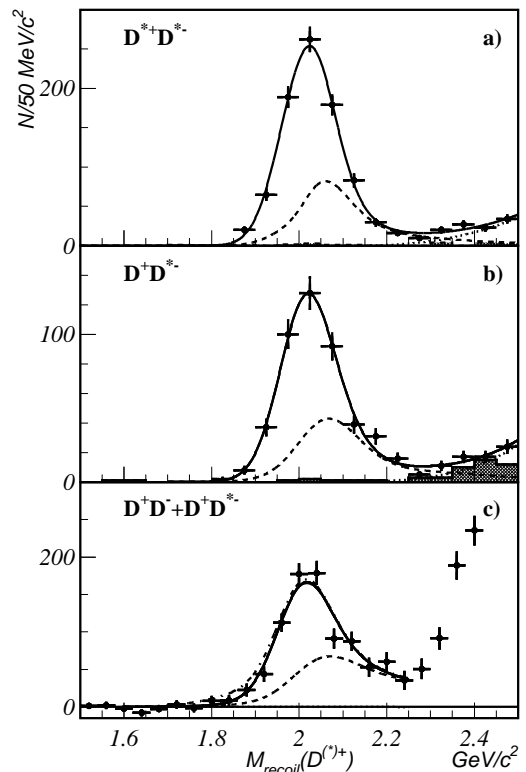


FIG. 1: a) $M_{\text{recoil}}(D^{*+})$ and b) $M_{\text{recoil}}(D^+)$ after applying the ΔM_{recoil} requirement. Points show the ΔM_{recoil} signal region; hatched histograms show the ΔM_{recoil} sideband; solid lines represent the fits described in the text; dashed lines show the contribution due to events with *ISR* photons of significant energy; dotted lines are the expected background contribution. c) $M_{\text{recoil}}(D^+)$ after D^+ sideband subtraction without requiring an extra π_{slow}^- in the event.

the MC predicts a contribution of 2.5 events from the signal process due to non-Gaussian tails in the $M_{D^{*+}}$ resolution function. The signal MC is normalized to the number of entries in the $M_{\text{recoil}}(D^{*+}) < 2.1 \text{ GeV}/c^2$ region in the data. Background (II) is estimated using the ΔM_{recoil} sideband ($0.150 \text{ MeV}/c^2 < \Delta M_{\text{recoil}} < 0.154 \text{ MeV}/c^2$). In the signal region 8 events are found; 4 events are expected according to MC from the signal process because of significant energy *ISR*. Thus backgrounds (I) and (II) are estimated to be smaller than 5 and 10 events at the 90% CL, respectively. The remaining background (III) can result in peaks in both the $M(D^{*+})$ and ΔM_{recoil} distributions, but has a threshold in the M_{recoil} distribution at $M_{D^{*+}} + M_{\pi^0} = 2.15 \text{ GeV}/c^2$, which is $\sim 1\sigma$ higher than the chosen M_{recoil} signal interval. To estimate the residual background (III) contribution in the signal region we perform a fit to the $M_{\text{recoil}}(D^{*+})$ distribution. The signal function is determined from the MC simulation and parametrized as the sum of a core Gaussian and an asymmetric function representing the case when the studied process is

accompanied by radiative photon(s) with significant energy ($E_{ISR} > 10$ MeV). The $M_{\text{recoil}}(D^{*+})$ resolution due to detector smearing and the signal function offset are left as free parameters in the fit to check the agreement with the MC predictions. The background (III) distribution is parameterized by a threshold function, $\alpha(M_{\text{recoil}}(D^{*+}) - M(D^{*-})_{PDG} - M(\pi^0)_{PDG})^\beta$, convolved with the detector resolution, where α and β are free parameters. The fit results are shown in the Fig. 1a as a solid curve; the dashed line shows the contribution of the studied process with significant energy *ISR* photons ($E_{ISR} > 10$ MeV). The dotted line represents the expected background (III) distribution. The signal yield is found to be 815 ± 28 events in the whole fit region (676 ± 24 events in the signal region $M_{\text{recoil}} < 2.1$ GeV/ c^2). The M_{recoil} resolution $\sigma = 56.1 \pm 2.2$ MeV/ c^2 is found to be in excellent agreement with the MC expectation (56.4 MeV/ c^2), and the shift of the signal peak position in the data with respect to the MC position is found to be consistent with zero (0.6 ± 2.5 MeV/ c^2). The contribution from background (III) in the signal region is estimated from this fit to be less than 2 events at the 90% CL.

For the process $e^+e^- \rightarrow D^+D^{*-}$, proceeding in a similar way, we find a signal yield of 423 ± 20 events in the whole fit region (360 ± 17 events in the signal region $M_{\text{recoil}} < 2.1$ GeV/ c^2), with backgrounds (I), (II) and (III) smaller than 8, 6 and 2 events at the 90% CL, respectively. Finally we estimate the total background in the $M_{\text{recoil}} < 2.1$ GeV/ c^2 interval to be smaller than 13 and 10 events for the $e^+e^- \rightarrow D^{*+}D^{*-}$ and $e^+e^- \rightarrow D^+D^{*-}$ processes, respectively, which is of the order of 1% of the signal. We therefore assume that all events in the interval $M_{\text{recoil}} < 2.1$ GeV/ c^2 are signal, and include the possible background contribution in the systematic error.

Since the reconstruction efficiency depends on the production and $D^{*\pm}$ helicity angle distributions, we perform an angular analysis before computing cross-sections. The helicity angle of the non-reconstructed D^{*-} is calculated assuming two-body kinematics. A scatter plot of the helicity angles for the two D^{*-} -mesons from $e^+e^- \rightarrow D^{*+}D^{*-}$ ($\cos\phi(D_{\text{rec}}^*)$ vs. $\cos\phi(D_{\text{non-rec}}^*)$) for the signal region is shown in Fig. 2a. This two dimensional distribution is fitted by a sum of three functions corresponding to the $D_T^*D_T^*$, $D_T^*D_L^*$ and $D_L^*D_L^*$ final states, obtained from the MC simulation. The fit finds 6_{-13}^{+15} , 708 ± 36 and 4_{-17}^{+18} events associated with $D_T^*D_T^*$, $D_T^*D_L^*$ and $D_L^*D_L^*$ final states, respectively. Figure 2b shows the D^{*-} meson helicity distribution for $e^+e^- \rightarrow D^+D^{*-}$. A fit finds 433 ± 24 and -1.5 ± 2 events corresponding to DD_T^* and DD_L^* , respectively. We conclude that in $e^+e^- \rightarrow D^{*+}D^{*-}$ and $e^+e^- \rightarrow D^+D^{*-}$ production the final states are saturated by $D_T^*D_L^*$ and DD_T^* . (DD_T^* is required by angular momentum and parity conservation for $e^+e^- \rightarrow D^+D^{*-}$ via a virtual photon; the $D_T^*D_L^*$ result is non-trivial.) The production angle distributions for $e^+e^- \rightarrow D_T^*D_L^*$ and $e^+e^- \rightarrow D^+D_T^*$ are, there-

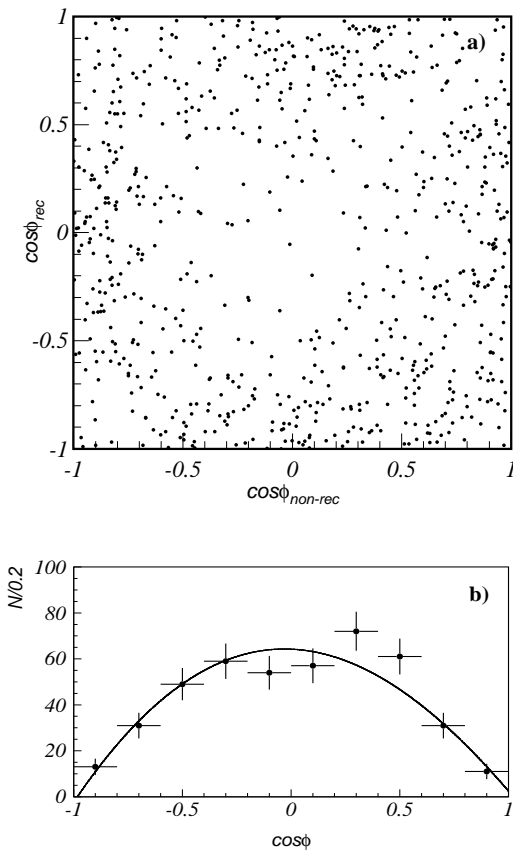


FIG. 2: a) A scatter plot of $\cos(\phi_{D_{\text{rec}}^*})$ vs. $\cos(\phi_{D_{\text{non-rec}}^*})$ for $e^+e^- \rightarrow D^{*+}D^{*-}$ events. b) D^{*-} meson helicity angle distribution for $e^+e^- \rightarrow D^+D^{*-}$ signal candidates. The curve represents the fit described in the text.

fore, fixed to be $1 + \cos^2\theta$ in both cases. As a cross-check we study the production angle distributions for D^{*+} from $e^+e^- \rightarrow D^{*+}D^{*-}$ and D^+ from $e^+e^- \rightarrow D^+D^{*-}$ processes. After correction for reconstruction efficiency in bins of the production angle we fit the production angle distributions with the function $(1 + A \cos^2\theta)$. The parameters A are found to be equal to $0.79_{-0.30}^{+0.34}$ and $2.3_{-0.7}^{+0.8}$ for the two processes, which are in agreement with the expected value $A = 1$ for both processes.

To calculate the Born cross-section for the studied processes we determine the fraction of events in the signal region with an *ISR* photon energy smaller than the chosen cutoff ($E_{\text{cutoff}} = 10$ MeV) using a MC simulation. In the MC we assume a $1/q^6$ dependence of the ratio of the cross section to $\sigma(e^+e^- \rightarrow \mu^+\mu^-)$ as predicted by Ref. [1]. We also try a $1/q^2$ dependence (corresponding to flat form-factors) and include the resulting shift of the event fraction ($< 1.3\%$) in the systematic error. The reconstruction efficiencies are determined from MC simulation. The Born cross-sections for $e^+e^- \rightarrow D^{(*)+}D^{*-}$ are calculated according to the formulae in Ref. [6] and

are listed in Table I. The final result is independent of the choice of E_{cutoff} . The sources of systematic error are summarized in Table II. The dominant contributions are from the uncertainties in tracking efficiency and $D^{(*)}$ branching ratios.

Process	σ_{Born} (pb)
$e^+e^- \rightarrow D_T^{*+}D_T^{*-}$	< 0.02 @ 90% CL
$e^+e^- \rightarrow D_T^{*+}D_L^{*-}$	$0.55 \pm 0.03 \pm 0.05$
$e^+e^- \rightarrow D_L^{*+}D_L^{*-}$	< 0.02 @ 90% CL
$e^+e^- \rightarrow D^+D_L^{*-}$	< 0.006 @ 90% CL
$e^+e^- \rightarrow D^+D_T^{*-}$	$0.62 \pm 0.03 \pm 0.06$
$e^+e^- \rightarrow D^+D^-$	< 0.04 @ 90% CL

TABLE I: The Born cross-section results. The first error is statistical and the second one is systematical.

TABLE II: Summary of systematic errors for the $e^+e^- \rightarrow D^{*+}D^{*-}$ and $e^+e^- \rightarrow D^+D^{*-}$ measurements.

Source	$e^+e^- \rightarrow D^{*+}D^{*-}$	$e^+e^- \rightarrow D^+D^{*-}$
Tracking efficiency	7%	5%
Identification	2%	2%
Backgrounds	$^{+0}_{-1.6}\%$	$^{+0}_{-2.5}\%$
Form-factor shape	1.3%	1.3%
Luminosity	1%	1%
$\mathcal{B}(D^{(*)})$	4%	8%
Total	9%	10%

We search for the process $e^+e^- \rightarrow D^+D^-$ by studying the mass spectrum of the system recoiling against the reconstructed D^+ without requiring an extra soft pion in the event. In the $e^+e^- \rightarrow D^{*+}D^{*-}$ and $e^+e^- \rightarrow D^+D^{*-}$ analyses, backgrounds are strongly suppressed by the ΔM_{recoil} cut, which is not applicable for the $e^+e^- \rightarrow D^+D^-$ search; without this requirement the combinatorial non- D^+ background is significant. We use D^+ mass sidebands ($20 \text{ MeV}/c^2 < |M_{K\pi\pi} - M_D| < 35 \text{ MeV}/c^2$) to extract the M_{recoil} distribution for the combinatorial background. Figure 1c shows the $M_{\text{recoil}}(D^+)$ distribution after D^+ mass sideband subtraction. We fit this distribution with the sum of two signal functions corresponding to D^- and D^{*-} peaks and a background function. The latter is a threshold function, $\alpha(x - M(D^-)_{PDG} - M(\pi^0)_{PDG})^\beta$, convolved with the detector resolution, where α and β are free parameters. For the fit we use only the region $M_{\text{recoil}} < 2.25 \text{ GeV}/c^2$, because of a possible contribution of $e^+e^- \rightarrow D^{(*)}D^{**}$ at higher M_{recoil} . The fit finds 13 ± 24 events in the D^- peak and 935 ± 42 in the D^{*-} peak. The fit function is shown in Fig. 1c as the solid line; the dashed line shows the contribution of events with *ISR* photons of significant energy (larger in this case due to the absence of the ΔM_{recoil} cut); and the dotted line represents the case where the contribution of $e^+e^- \rightarrow D^+D^-$ is set at the value corresponding to the 90% CL upper limit. The reconstruction

efficiencies for $e^+e^- \rightarrow D^+D^-$ and $e^+e^- \rightarrow D^+D^{*-}$ are found from MC. The production angle distribution for $e^+e^- \rightarrow D^+D^-$ is assumed to be proportional to $\sin^2\theta$, while the production angle for $e^+e^- \rightarrow D^+D^{*-}$ is fixed from the study with the ΔM_{recoil} requirement. The $e^+e^- \rightarrow D^+D^{*-}$ Born cross-section is calculated to be 0.54 ± 0.04 pb. In this method the systematic uncertainty in the signal yield is larger than in the ΔM_{recoil} method due to significant $e^+e^- \rightarrow D^+D\pi$ background under the peak, which can only be extrapolated from the higher M_{recoil} region with large uncertainties. For the $e^+e^- \rightarrow D^+D^-$ Born cross-section we set an upper limit of 0.04 pb at the 90% CL.

The relative sizes of the measured cross-sections agree with the predictions of Ref. [1]: $\sigma(e^+e^- \rightarrow D_T^{*+}D_L^{*-})$ and $\sigma(e^+e^- \rightarrow D^+D_T^{*-})$ are similar, while $\sigma(e^+e^- \rightarrow D^+D^-)$ is much smaller. $e^+e^- \rightarrow D^{*+}D^{*-}$ production is saturated by the $D_T^{*+}D_L^{*-}$ final state, also as expected. The absolute cross-sections are smaller than those of [1] by a factor of 4, which is comparable to the theoretical uncertainty. Recent calculations based on the constituent quark model [3] reproduce the $D^{*+}D^{*-}$ and D^+D^{*-} cross-sections very well, but predict $\sigma(e^+e^- \rightarrow D^+D^-) = 0.1$ pb, somewhat larger than our limit. The predicted $D_L^{*+}D_T^{*-}$ fraction in $e^+e^- \rightarrow D^{*+}D^{*-}$ production, 65% [3], is smaller than we observe.

In summary, we report the first measurement of the cross-sections for the $e^+e^- \rightarrow D_T^{*+}D_L^{*-}$ and $e^+e^- \rightarrow D^+D_T^{*-}$ processes at $\sqrt{s} = 10.6 \text{ GeV}$ and set upper limits on the $e^+e^- \rightarrow D_T^{*+}D_T^{*-}$, $e^+e^- \rightarrow D_L^{*+}D_L^{*-}$, $e^+e^- \rightarrow D^+D_L^{*-}$ and $e^+e^- \rightarrow D^+D^-$ cross-sections.

We are grateful to A.G.Grozin for useful discussion and comments on theoretical issues.

We wish to thank the KEKB accelerator group for the excellent operation of the KEKB accelerator. We acknowledge support from the Ministry of Education, Culture, Sports, Science, and Technology of Japan and the Japan Society for the Promotion of Science; the Australian Research Council and the Australian Department of Education, Science and Training; the National Science Foundation of China under contract No. 10175071; the Department of Science and Technology of India; the BK21 program of the Ministry of Education of Korea and the CHEP SRC program of the Korea Science and Engineering Foundation; the Polish State Committee for Scientific Research under contract No. 2P03B 01324; the Ministry of Science and Technology of the Russian Federation; the Ministry of Education, Science and Sport of the Republic of Slovenia; the National Science Council and the Ministry of Education of Taiwan; and the U.S. Department of Energy.

* on leave from Nova Gorica Polytechnic, Nova Gorica

- [1] A.G. Grozin, M. Neubert, *Phys. Rev. D* **55**, 272 (1997).
- [2] A.G. Grozin, private communications.
- [3] K.-Y. Liu *et al.*, hep-ph/0311364.
- [4] A. Abashian *et al.*, *Nucl. Instrum. Methods A* **479**, 117 (2002).
- [5] S. Kurokawa and S. Kikutani *Nucl. Instrum. Methods A* **499**, 1 (2003).
- [6] E.A. Kuraev, V.S. Fadin, *Yad. Phys.* **41**, 733-742 (1985).